# Numerical investigation of hydroacoustic pressure pulsations due to rotor-stator interaction in the Francis-99 turbine

**D Platonov[1,2], A Minakov[1,2], A Sentyabov[1,2]**

[1] Siberian Federal University, Krasnoyarsk, Svobodniy 79, 660079 Russia
[2] Institute of Thermophysics SB RAS, Novosibirsk, Lavrentyeva 1, 630090 Russia

E-mail: platonov-08@yandex.ru, tov-andrey@yandex.ru, sentyabov_a_v@mail.ru

**Abstract**. The paper deals with the numerical simulation of the flow in the Francis-99 hydraulic turbine at three different problem formulations, namely, the application of the method of rotating coordinate system, sliding mesh model, and consideration of a compressible fluid. The pulsations intensity and pressure pulsation spectra obtained by numerical simulation and experimentally are compared. It is shown that the simulation of a problem considering compressible fluid, and that conducted by the sliding mesh method gives significantly greater pressure amplitudes. It is also shown that the precessing vortex core is a source of pressure waves in the entire turbine flow path.

**Keywords:** Francis turbine, numerical simulation, pressure pulsation, the precession of the vortex rope, turbulence, CFD, LES, hydroacoustic.

## 1. Introduction

Due to the compressibility of water, pressure waves propagate in it at a finite velocity. Therefore, in the hydraulic turbine flow path, which can be represented as a system of channels, acoustic (hydroacoustic) pulsations can be generated. In the case of presence of hydrodynamic, mechanical, electrical, seismic, and other types of perturbations with frequencies close to the eigenfrequencies of the hydroacoustic system, resonant phenomena can occur in the turbine flow path, leading to increased vibrations and even to emergency situations. Therefore, the calculation of hydroacoustic pulsations in the turbine flow path is of great importance.

## 2. Numerical simulation

When describing the hydroacoustic phenomena in the hydraulic turbines flow path one faces several problems. The first problem consists in the need to take into account the compressibility of water. To calculate the compressibility, it is necessary to have the equation of state $P=f(\rho)$. Currently, there are a large number of different equations of state for water [1]. In this paper, the Tate equation (1) of state was used, which can be written as:

$$1+\frac{n}{K}\left(P-P_0\right)=\left(\frac{\rho}{\rho_0}\right)^n \tag{1}$$

here $\rho$ is the density of the liquid at pressure $P$; $n$ is the compressibility index; $K$ is the elasticity modulus of water; $P_0$ and $\rho_0$ are the pressure and density of the liquid under normal conditions.

The elasticity modulus of the liquid is $K=a^2\rho$, where $a$ is the sound velocity.

**Добавлено примечание ([SAV1]):** обычно давление маленькой буквой обозначают. К тому же, ниже давление обозначено маленькой буквой

The second problem is related to the need to simulate turbulence in the channels of complex geometric shape, as well as a strong flow swirling.

The swirled flow in the hydraulic turbine may be accompanied by the precession of the vortex core. To simulate this phenomenon, it is necessary to use non-stationary, in particular, vortex-resolving methods, such as for example Large Eddy Simulation (LES).

The third problem, when simulating hydraulic turbines, is related to the need to take into account the rotation of the runner and the interaction of the rotor-stator. There are several approaches to simulate flows with rotating bodies. They include a sliding mesh method and a method based on the transition to a rotating coordinate system. The most common and simple way to simulate the rotation of the impeller is to use a rotating coordinate system. The transition to a rotating coordinate system makes it possible to simulate the flow in the approximation, in which the runner is stationary, while the swirling liquid flows onto it. This approach is often called a *frozen rotor*. However, this problem formulation does not take into account the rotor-stator interaction, and as a result, may not always correctly reproduce the vortex structure of the flow and pressure pulsations caused by the precession of the vortex core.

Below are the basic equations of the mathematical model of hydroacoustic processes, expressing the conservation laws in a rotating coordinate system.

The equation of continuity (mass conservation law):

$$\frac{\partial \rho}{\partial t} + \nabla(\rho \mathbf{v}) = 0 \tag{2}$$

The momentum equation (momentum conservation law) in the rotating reference frame for relative velocities:

$$\frac{\partial \rho \mathbf{v}}{\partial t} + \nabla(\rho \mathbf{v} \cdot \mathbf{v}) = -\nabla p + \nabla(\boldsymbol{\tau}^m + \boldsymbol{\tau}^t) + (\rho - \rho_0)\mathbf{g} - \rho(2\boldsymbol{\Omega} \times \mathbf{v} + \boldsymbol{\Omega} \times (\boldsymbol{\Omega} \times \mathbf{r})) \tag{3}$$

where $\mathbf{v}$ is the fluid velocity vector, $\boldsymbol{\tau}$ is the viscous tension tensor, $\boldsymbol{\Omega}$ is the angular velocity vector of rotation of the runner, $p$ is the static pressure, and $\rho$ is the density. When transiting to a rotating coordinate system, the right part of the momentum conservation equation is supplemented by the Coriolis force and the centrifugal force.

The components of the viscous stress tensor $\tau^m$ are defined as:

$$\tau_{ij}^m = \mu \left[ \left( \frac{\partial u_i}{\partial x_j} + \frac{\partial u_j}{\partial x_i} \right) - \frac{2}{3} \delta_{ij} \frac{\partial u_k}{\partial x_k} \right] \tag{4}$$

where $\mu$ is the dynamic (molecular) viscosity, $u_i$ are the velocity vector components, $\delta_{ij}$ is the Kronecker symbol.

The numerical simulation technique is considered in more detail in [2-4].

In this work, it is planned to conduct a study considering the flow in the Francis-99 turbine, determining the influence of the medium compressibility on the pressure pulsations and the flow pattern under certain operating conditions using the sliding mesh model.

**3. Algorithm testing**

First, it is necessary to test a numerical simulation technique for the case of a compressible fluid. The analysis has shown that the problem of hydraulic shock can be considered as the most reliable and close to the conditions of the flow path tests. As a test task, the experiment shown in Fig. 1 was chosen [7].

The pipeline length in this experiment was 98.11 m, which is comparable to the penstock lengths of high-head hydroelectric power plants. In addition, in this task, the penstock was under pressure of 1250 kPa, which is also comparable to the liquid pressure at a height of 120-200 m typical for high-

**Добавлено примечание ([SAV2]):** вроде, обычно в абсолютной формулировке считаем

head hydroelectric power plant. From the lower reservoir, water enters the upper reservoir through a pipeline with a diameter of 16 mm and a length of $L$=98.11 m. The superficial velocity of the liquid in the pipe is 0.94 m/s, which corresponds to the Reynolds number of 15,800. Further, at some point in time, almost instantly (0.003 s), the valve at the end of the pipe is sharply shut down that causes the emergence of hydraulic oscillations in the pipe. The pressure change over time is recorded at four points of the pipe by the pressure transducers installed as shown in the diagram of Fig. 4.

**Добавлено примечание ([SAV3]):** не могу понять, что это значит

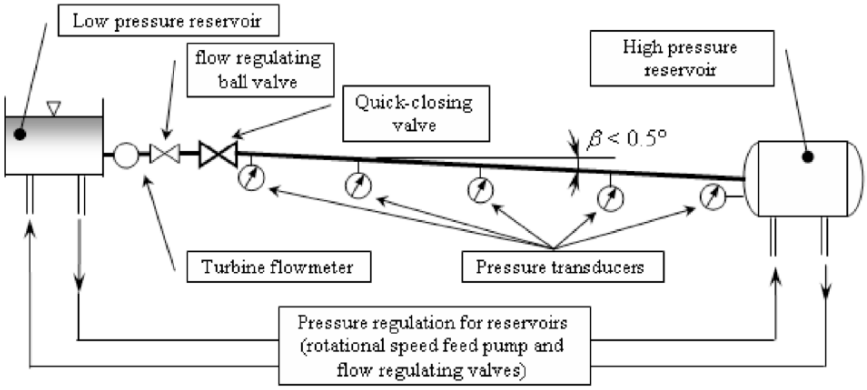


**Figure 4.** Schematic set-up

Simulation of this problem was carried out in the spatial formulation. The used calculation mesh contained 1,000 nodes along the length and 10 nodes along the radius of the pipeline. The time step was equal to 0.0005 s.

Hydroacoustic pressure waves are formed in the pipe. Figure 5 shows the pressure distribution along the pipe at different time points. The beginning of the X-axis corresponds to the inlet reservoir. The right end of the graph coincides with a solid wall at the location of the shut valve. The pressure in the high-pressure reservoir was 1250 kPa. Sound wave speed in the liquid was 1319 m/s.

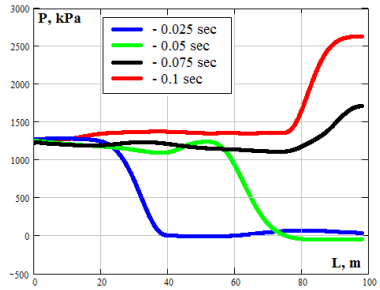


**Figure 5.** Distribution of static pressure in the pipe at different time points.

Comparison of the design pressure with the readings of experimental transducers at four points along the flow path is shown in Figs. 6-9. As can be seen, there is a good agreement between the calculation and experiment on the amplitude, frequency, and the rate of pulsations attenuation. It can

be seen that in both calculation and experiment gradual attenuation of pressure pulsations amplitude in time is observed. This attenuation is caused by the effect of viscosity.

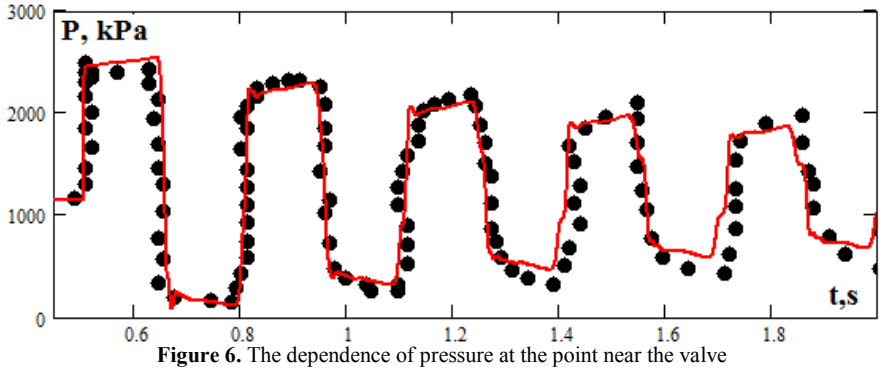


**Figure 6.** The dependence of pressure at the point near the valve
(black points show experimental results, red line show calculation results)

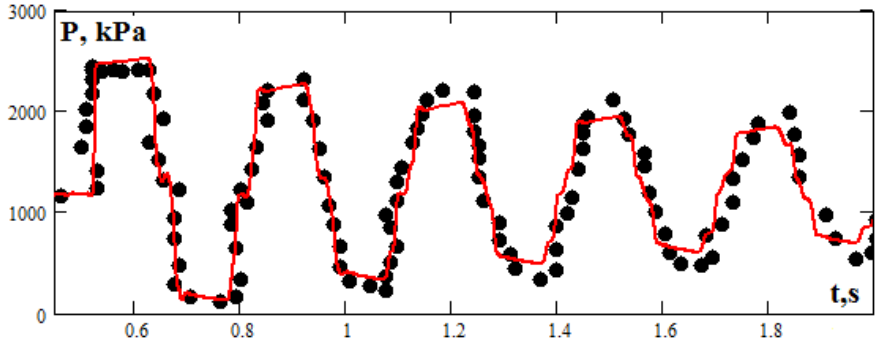


**Figure 7.** The dependence of pressure at the point at a distance of 0.25$L$ from the valve
(black points show experimental results, red line show calculation results)

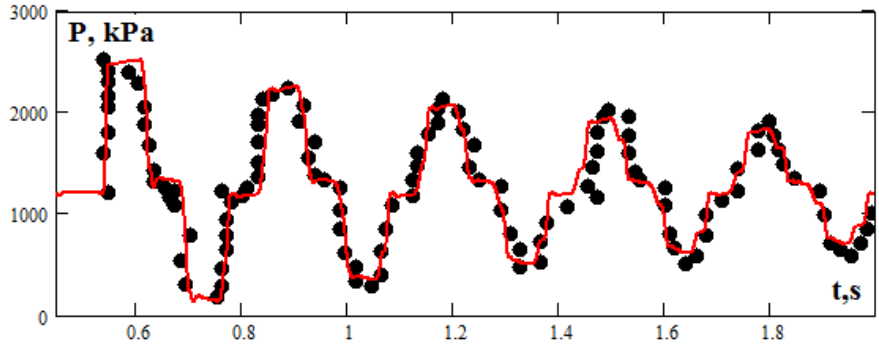


**Figure 8.** The dependence of pressure at the point at a distance of 0.5$L$ from the valve
(black points show experimental results, red line show calculation results)

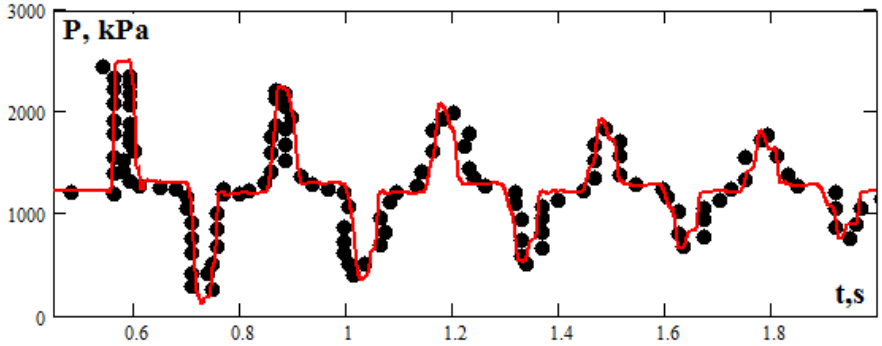


**Figure 9.** The dependence of pressure at the point at a distance of 0.75*L* from the valve (black points show experimental results, red line show calculation results)

**4. Simulation observation**

Next, a study was conducted according to the proposed numerical calculation technique for one of the operation modes of the Francis-99 hydraulic unit at four different problem formulations: 1) incompressible fluid, the frozen rotor method; 2) incompressible fluid, sliding mesh model; 3) compressible fluid taking into account hydroacoustic vibrations, the frozen rotor method; and 4) compressible fluid taking into account hydroacoustic vibrations, sliding mesh model.

The *part load (PL) performance* was chosen for the study. As a rule, such modes are accompanied by a pronounced vortex structure and, as a consequence, the maximum level of pressure pulsations.

The computations have been carried out using an unstructured grid with the total number of 5.12 million nodes for the whole domain. This grid detailing is sufficient for this task; this was shown in work [8]. The time step was chosen from the Courant condition and was $3 \cdot 10^{-4}$ seconds for this task.

Figure 10 shows the instantaneous vortex structure behind the runner for a fixed pressure. It can be concluded from the figures that for the problem formulation of compressible fluid and sliding mesh model, the pressure amplitude is much larger, while the vortex structure is expressed much stronger.

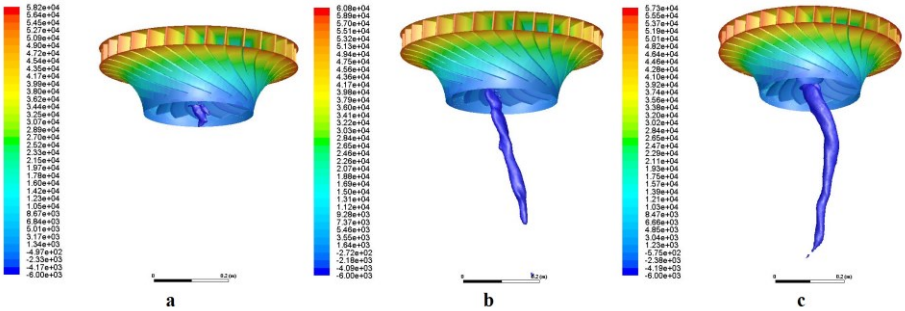


**Figure 10.** Vortex structure in the *PL* regime for different models, ***P*** *= 6 kPa:*
*(a – frozen rotor method, incompressible fluid; b – sliding mesh model, incompressible fluid; c - frozen rotor method, compressible fluid)*

The most interesting in this work is the analysis of the behaviour of acoustic fields. The structure of acoustic pulsations is most clearly shown by the time derivative of the liquid density. Figure 11 shows

the distribution of the derivative of density on the turbine walls and in the central section of the spiral case depending on time. Analysis of the calculated data shows that in the turbine under consideration there are several sources of acoustic pressure waves. First, Fig. 11b clearly shows that the main source of high-frequency pulsations is the interaction between the rotor and the stator. The rotating runner generates radially diverging pressure waves. These waves are reflected from the guide vanes and column of the spiral case. Pressure waves, generated by the runner, after having interacted with the guide vane assembly, propagate up and down the turbine flow path. Pulsations caused by the interaction of the rotor and the stator have high frequencies. This is clearly seen by the short-wave structure in Fig. 11.

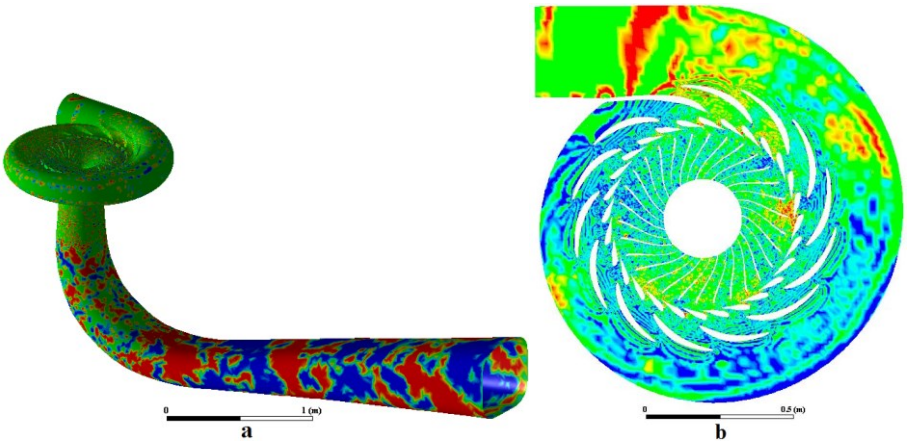


**Figure 11.** Distribution of the time derivative of density on the turbine walls, and the central section of the spiral case.

Another source of acoustic pressure waves in the turbine is a precessing vortex core. Figure 12 shows the precession dynamics of the vortex core and the pressure wave, which are generated by these pulsations. It is seen that the vortex core generates pressure waves diverging parallel to its surface.

At that, low-frequency pressure waves caused by fluctuations in flow rate in the flow path superimpose on these pulsations. The structure of these long-wavelength waves is clearly visible on the walls of the draft tube (Fig. 11a).

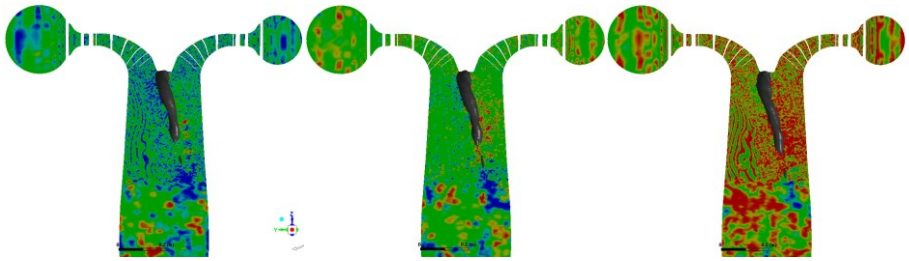

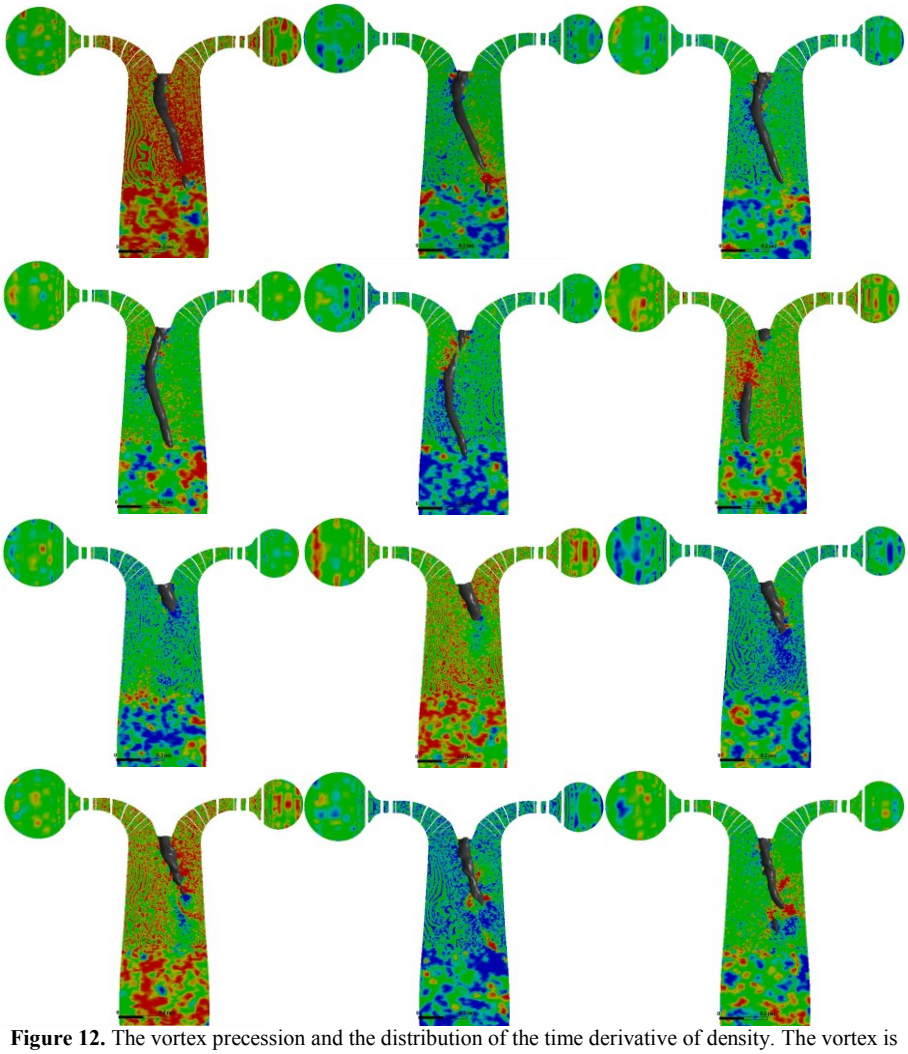

**Figure 12.** The vortex precession and the distribution of the time derivative of density. The vortex is shown by the pressure iso-surface.

Figure 13 shows the pulsations and the pressure pulsation spectrum for three different problem formulations compared to the experiment. The monitoring point is located behind the runner in the draft tube diffuser near the wall (DT5). From the presented data, one can estimate the contribution of various phenomena to the overall pressure pulsations. Thus, three components of pressure pulsations can be clearly traced. These are low-frequency pulsations associated with the vortex precession, which are visible at all problem formulations, as well as high-frequency pulsations associated with rotor-stator interaction and fluid compressibility.

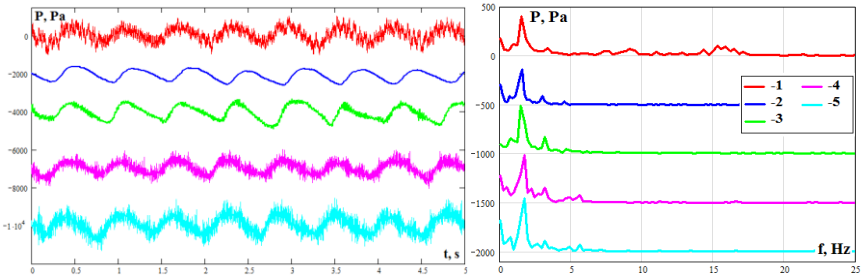


**Figure 13.** The pressure pulsations and spectrum of pressure pulsations at the DT5 point for *PL* regime *(1- experiment; 2- incompressible liquid, "frozen rotor"; 3- compressible liquid, "frozen rotor"; 4- incompressible liquid, slide mesh; 5- compressible liquid, slide mesh).*

As it is obvious, the calculations for various problem formulations, give in general fairly close results both in amplitude and the frequency of the pulsations. A significant difference is observed only in the compressible problem formulation with the sliding mesh model. In this problem formulation, high-frequency pulsations associated with the interaction of the rotor-stator are clearly manifested. These pulsations in the considered mode are obviously the most intense. Pulsations associated with the fluid compressibility are traced as well. They also have a high-frequency component, but appear in the draft tube, as it is seen, much weaker than the pressure pulsations associated with the interaction of the rotor and the stator.

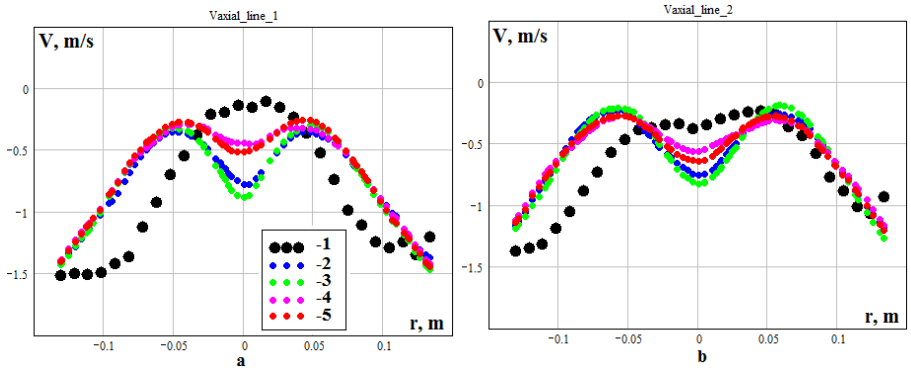


**Figure 14.** The axial component of the velocity in line 1 (a) and line 2 (b) for PL regime *(1- experiment; 2- incompressible liquid, "frozen rotor"; 3- compressible liquid, "frozen rotor"; 4- incompressible liquid, slide mesh; 5- compressible liquid, slide mesh)*

The analysis of the influence of different problem formulations on the calculation accuracy of the averaged velocity fields did not reveal a significant effect. As can be seen from Fig. 14, all problem formulations give very close results. On average, the results obtained at a compressible fluid formulation with the sliding mesh model are closer to the experimental data.

## 5. Conclusions

The paper presents the numerical simulation of the flow in the Francis-99 hydraulic turbine for three different problem formulations, namely, the frozen rotor method, sliding mesh model, and consideration of a compressible fluid. The problem of hydroacoustic pulsations in a long pipeline is

considered as a test. In consequence of testing, a good agreement of calculations and experiments on the hydroacoustic pressure pulsations amplitude and frequency was obtained. The described hydroacoustic simulation technique was tested through the calculation of pressure pulsations in the Francis-99 turbine flow path. It is shown that the simulation at the problem formulation based on compressible fluid, and the sliding-mesh model gives a significantly higher pressure amplitude. It is also revealed that the precessing vortex core is a source of acoustic pressure waves in the draft tube.

The pulsations and pressure pulsation spectra obtained by simulation and experimentally were compared, and the contribution of various phenomena to the total pressure pulsations was estimated. It is shown that the main low-frequency pressure pulsations in the draft tube are associated with the vortex precession. The main high-frequency pressure pulsations are associated with rotor-stator interaction. High-frequency pulsations associated with the liquid compressibility are much weaker than the pressure pulsations associated with the interaction of the rotor and the stator.

Comparison of the simulation results with the experimental data has shown that the best results can be achieved using a compressible fluid model, as well as a sliding mesh model.

**Добавлено примечание ([SAV4]):** уточнить,

**Acknowledgement**

The reported study was funded by RFBR and the government of Krasnoyarsk region according to the research project № 18-48-242007 р_мк.

**Добавлено примечание ([SAV5]):** кириллица!

**References**

[1] Abovsky, V. A.,. On the Tate equation of state. *High Temperature*, 1972, vol. 10, 6, pp. 14-22.

[2] Minakov, A.V., Platonov, D.V., Dekterev, A.A., Sentyabov, A.V., and Zakharov, A.V., 2015. The analysis of unsteady flow structure and low-frequency pressure pulsations in the high-head Francis turbines. *International Journal of Heat and Fluid Flow,* **53,** pp. 183-194.

[3] Minakov, A.V., Platonov, D.V., Dekterev, A.A., Sentyabov, A.V., and Zakharov, A.V., 2015. The numerical simulation of low-frequency pressure pulsations in the high-head Francis turbine *Computers and Fluids,* **111, April,** pp. 197 – 205. doi:10.1016/j.compfluid.2015.01.007

[4] Minakov, A.V., Platonov, D.V., Litvinov, I.V., Shtork, S.I., Hanjalić, K., 2017. Vortex ropes in the draft tube of a laboratory Kaplan hydro turbine at low load: an experimental and LES scrutiny of RANS and DES computational models. *Journal of Hydraulic Research.* Vol. **55**, 5, pp. 668-685.

[5] Smirnov, R., Shi, S., Celik, I., 2001. Random flow generation technique for large-eddy simulations and particle-dynamics modeling. *J. Fluids Engineering,* **123,** pp. 359-371.

[6] Picano, S., and Hanjalić, K., 2012. Leray-α regularization of the Smagorinsky-closed filtered equations for turbulent jets at high Reynolds numbers. *Flow, Turbulence and Combustion*, **89**, pp. 627-650.

[7] Adamkowski, A., Lewandowski, M., 2006. Experimental examination of unsteady friction models for transient pipe flow simulation. *Journal of Fluids Engineering*, Nov., vol. 128, pp. 1351-1363.

[8] Minakov, A., Platonov, D., Sentyabov, A., Gavrilov, A., 2017, Francis-99 turbine numerical flow simulation of steady state operation using RANS and RANS/LES turbulence model *Journal of Physics: Conference Series,* **782**, Issue 1, 012005